DOI: 10.1002/ ((please add manuscript number))

Article type: Full Paper

Reduced Graphene Oxide-GelMA Hybrid Hydrogels as Scaffolds for Cardiac Tissue Engineering

Su Ryon Shin[1,2,3], Claudio Zihlmann[1,2], Mohsen Akbari[1,2,4], Pribpandao Assawes[1,2], Louis Cheung[5], Kaizhen Zhang[6], Vijayan Manoharan[1,2], Yu Shrike Zhang[1,2], Mehmet Yüksekkaya[7], Kai-tak Wan[6], Mehdi Nikkhah[8], Mehmet R. Dokmeci[1,2,3], Xiaowu (Shirley) Tang[5], Ali Khademhosseini[1,2,3,9,10] **

[1]Biomaterials Innovation Research Center, Department of Medicine, Brigham and Women's Hospital, Harvard Medical School, Cambridge, MA 02139, USA.

[2]Harvard-MIT Division of Health Sciences and Technology, Massachusetts Institute of Technology, Cambridge, MA 02139, USA.

This is the author manuscript accepted for publication and has undergone full peer review but has not been through the copyediting, typesetting, pagination and proofreading process, which may lead to differences between this version and the Version of Record. Please cite this article as doi: 10.1002/smll.201600178.

This article is protected by copyright. All rights reserved.

This is the author manuscript accepted for publication and has undergone full peer review but has not been through the copyediting, typesetting, pagination and proofreading process, which may lead to differences between this version and the Version of Record. Please cite this article as doi: 10.1002/smll.201600178.

This article is protected by copyright. All rights reserved.

[3]Wyss Institute for Biologically Inspired Engineering, Harvard University, Boston, MA 02139, USA.

[4]Department of Mechanical Engineering, University of Victoria, 3800 Finnerty Rd., Victoria, BC, V8P 2C5, Canada.

[5]Department of Chemistry & Waterloo Institute for Nanotechnology, University of Waterloo, 200 University Ave. West, Waterloo, Ontario, N2L 3G1, Canada.

[6]Department of Mechanical and Industrial Engineering, Northeastern University, Boston, Massachusetts 02115, USA.

[7]Faculty of Engineering, Biomedical Engineering Department, Baskent University, Ankara, Turkey.

[8]School of Biological and Health Systems Engineering, Arizona State University, Tempe, AZ, 85251, USA.

[9]Department of Physics, King Abdulaziz University, Jeddah 21569, Saudi Arabia.

[10]College of Animal Bioscience and Technology, Department of Bioindustrial Technologies, Konkuk University, Hwayang-dong, Kwangjin-gu, Seoul 143-701, Republic of Korea

CORRESPONDING AUTHOR

Biomaterials Innovation Research Center, Brigham and Women's Hospital, Harvard Medical School. Cambridge, MA, USA. 02139.

E-mail address: alik@bwh.harvard.edu (A. Khademhosseini)

This article is protected by copyright. All rights reserved.

Author Manuscript

This article is protected by copyright. All rights reserved.

Department of Chemistry, University of Waterloo, Waterloo, Ontario N2L 3G1, Canada.

E-mail address: tangxw@uwaterloo.ca (Xiaowu (Shirley) Tang)

Keywords: reduced graphene oxide, gelatin, hydrogel, cardiac tissue engineering, bioactuator

Abstract

Biomaterials currently used in cardiac tissue engineering have certain limitations, such as lack of electrical conductivity and appropriate mechanical properties, which are two parameters playing a key role in regulating cardiac cellular behavior. In this work, we engineered myocardial tissue constructs based on reduced graphene oxide (rGO)-incorporated gelatin methacrylyol (GelMA) hybrid hydrogels. The incorporation of rGO into the GelMA matrix significantly enhanced the electrical conductivity and mechanical properties of the material. Moreover, cells cultured on composite rGO-GelMA scaffolds exhibited better biological activities such as cell viability, proliferation, and maturation compared to ones cultured on GelMA hydrogels. Cardiomyocytes showed stronger contractility and faster spontaneous beating rate on rGO-GelMA hydrogel sheets compared to those on pristine GelMA hydrogels, as well as GO-GelMA hydrogel sheets with similar

This article is protected by copyright. All rights reserved.

Author Manuscript

This article is protected by copyright. All rights reserved.

mechanical property and particle concentration. Our strategy of integrating rGO within a biocompatible hydrogel is expected to be broadly applicable for future biomaterial design to improve tissue engineering outcomes. The engineered cardiac tissue constructs using rGO incorporated hybrid hydrogels can potentially provide high-fidelity tissue models for drug studies and the investigations of cardiac tissue development and/or disease processes *in vitro*.

1. Introduction

Cardiac tissue injury, such as the traumatic damage caused by myocardial infarction or coronary artery disease, is one of the leading causes of death globally[1, 2]. Since myocardial tissue lacks intrinsic regenerative capacity, the damage induced by cardiac injury is permanent, and there are very few treatment options[2]. Heart transplantation is currently the only long-term strategy for treatment of large-scale cardiac injuries. However, the number of donors are limited, and only a small fraction of patients on transplant waiting lists can receive a new heart. Recently, significant efforts have been made to engineer cardiac tissue "patches" as synthetic transplants to replace areas of damaged myocardial tissue, but several issues persist[3, 4]. For example, since the size of the infarct damage varies greatly, the engineered replacement tissues should be able to reestablish the structure and function of native tissues across different size scales. In addition, cardiac tissues require specific contractile properties that are directly related to cellular orientation and elongation.

This article is protected by copyright. All rights reserved.

Author Manuscript

This article is protected by copyright. All rights reserved.

It remains a great challenge to engineer cardiac tissues that simulate the microarchitecture of the native myocardium, in terms of topographical features, biophysical and mechanical properties.

Development of scaffolds that mimic the natural extracellular matrix (ECM) is of great interest in myocardial tissue engineering. The ECM plays a crucial mechanical role and is fundamental to having a functional cardiac muscle. It provides the structural foundation for the myocardium and creates an ideal microenvironment for cells to function. The main components of the myocardial ECM are collagen types I and III that are synthesized by cardiac fibroblasts[5]. Other components include laminin, fibronectin and glycoproteins. These additional components are important for cell adhesion and cell-cell interactions[6]. One strategy to fabricate biomimetic scaffolds is to use native ECM components including collagen[7], fibrin[8] or laminin[9]. These scaffolds have been seeded with cardiomyocytes, which show continuous, rhythmic, and synchronized contractions[9]. These materials exhibit predictable and reproducible mechanical properties and degradation rates, which allows tailoring of their biophysical properties to match those of natural tissue. The main advantage of using naturally-derived polymers in scaffolds is that they often result in reduced inflammatory response when integrated with the host tissue compared with synthetic polymers such as polyglycolic acid (PGA)[9], polycaprolactone (PCL)[10], and poly(glycerol sebacate) (PGS)[11] [12].

Despite the excellent biocompatibility of naturally-derived polymers, their poor mechanical properties and nascent electrical conductivity have hampered their applications in engineering of cardiac tissues. For example, in terms of mechanical properties, the tissue scaffolds require material

This article is protected by copyright. All rights reserved.

Author Manuscript

This article is protected by copyright. All rights reserved.

stiffness in the range of 5-150 kPa[11]. One potential approach is to create a hybrid hydrogel scaffold that is formed by adding reinforcing materials to a natural polymer matrix. Several recent studies have shown that conductive scaffolds are preferred over insulating polymer counterparts for myocardial tissue engineering applications [3, 13, 14]. Carbon nanomaterials, especially carbon nanotube (CNT) and graphene, are considered promising reinforcing materials for such purposes, due to their excellent physical properties such as their high mechanical strength and unique electrical conductivity[15]. We have recently showed that cardiomyocytes seeded on CNT-gelatin methacrylyol (GelMA) hybrid hydrogel matrix exhibited stronger synchronous beating behaviour and higher spontaneous beating rates compared to those cultured on pure GelMA [16].

Recently, graphene and its derivatives such as graphene oxide (GO) and reduced graphene oxide (rGO) have emerged as a new class of nanomaterials for several biomedical applications including drug delivery, cell imaging, and as tissue scaffolds[17]. One potential concern is the cellular toxicity of these materials after degraded hydrogel matrix such as GelMA. It has been shown that the cytotoxicity of these nanoparticles depends on their shape and composition[18]. For example, two-dimensional (2D) graphene exhibits lower cytotoxicity compared to one-dimensional (1D) CNTs [19, 20]. GO is usually preferred over graphene for producing homogeneous aqueous suspensions due to the oxygen-containing groups on its basal plane (hydroxyl and epoxide groups) and edges (carboxyl groups), which make the GO sheets very hydrophilic[21]. However, GO exhibits relatively low electrical conductivity compared to graphene sheets[22]. In addition, the cellular behavior on the

This article is protected by copyright. All rights reserved.

Author Manuscript

This article is protected by copyright. All rights reserved.

reduced version of materials based on GO (i.e., rGO) can be regulated by tuning the surface oxygen content of rGO[19]. Specifically, it has been shown that cell adhesion and proliferation are enhanced on partially reduced GO, which may be induced by enhanced adsorption of ECM proteins on rGO surface by non-covalent interactions. Furthermore, rGO-based hybrid or composite hydrogel such as rGO incorporated collagen scaffold[23], polymer core-reduced graphene oxide shell nanofiber mat (rGO/CSNFM)[24], rGO/polypeptide thermogel (rGO/P)[25], and rGO/sodium carboxymethyl cellulose (CMC)/silk fibroin (SF) nanocomposite matrix[26] have been shown the high cell viability and nontoxicity properties with enhanced mechanical or electrical properties. Therefore, rGO is a promising material for cardiac tissue engineering applications.

Here, we present a hybrid hydrogel, which is composed of rGO nanoparticles homogeneously dispersed into a GelMA hydrogel scaffold. In order to improve the electrical properties of GO, GO sheets were reduced using ascorbic acid, which was not only a biocompatible reducing agent[27] but also prevented the apoptosis of cardiomyocytes and induced the differentiation of embryonic stem cells into cardiomyocytes[28]. GelMA is a chemically modified gelatin which is a denatured form of collagen. It was used as a base material because of its excellent biocompatibility and the presence of cell binding moieties[29]. In addition, gelatin chains have been used to reduce GO and prevent aggregation of GO in suspension.[22, 30] Therefore, rGO can be easily incorporated into the GelMA hydrogel matrix to improve the mechanical and electrical properties of the hydrogel, which would lead to a more natural microenvironment for the cardiomyocytes and thus induce improved cardiac tissue morphogenesis and beating behavior.

This article is protected by copyright. All rights reserved.

Author Manuscript

This article is protected by copyright. All rights reserved.

2. Results and Discussion

Conventional fabrication methods used for generating rGO require high or low pH solutions, high temperature (> 90 °C) and toxic reductants such as hydrazine which are not compatible with cell studies. In this work, we used ascorbic acid, a naturally occurring organic compound, to reduce rGO from GO at 80 ^{o}C[27] (**Schematic 1 A**). Change in the color of the solution was used as an indicator on successful reduction of GO. While the color of the initial GO solution was brownish, it turned to black after the reduction process **(Figure 1A)**. The FTIR spectrum of GO **(Figure 1B)** showed characteristic peaks at 3448 cm^{-1} (O-H stretching), 2957, 2923, 2854 cm^{-1} (CH_2, CH_3 stretching), 1720 cm^{-1} (C=O stretching), 1630 cm^{-1} (C=C stretching), 1399 cm^{-1} (O-H bending), 1260 cm^{-1} (C-OH stretching) and 1055 cm^{-1} (C-O-C stretching). After reduction, the peak at 1720 cm^{-1} that corresponds to C=O stretching disappeared, and the peaks in the fingerprint region from 1500 to 1000 cm^{-1} became weaker due to the removal of oxygen-containing groups. The persistently large peak at 3448 cm^{-1} in the FTIR spectrum of rGO was mostly due to the moisture contained in the KBr pellets which could not be avoided. To further characterize the effect of GO reduction, we performed X-ray photoelectron spectroscopy (XPS) measurements for more information. XPS results showed that the content of oxygen groups in the GO and rGO were vastly different. The GO showed lower C/O ratio (2.75:1) than rGO (5.2:1), which was calculated by the areas under the C_{1s} and O_{1s} peaks after factoring in the photo-ionization cross-section (**Figure 1C**). The positions of the peaks of GO were

This article is protected by copyright. All rights reserved.

Author Manuscript

This article is protected by copyright. All rights reserved.

284.5 eV (C=C sp^2-hybridized carbon, and C-C sp^3-hybridized carbon), 286.6 eV (C-OH/C-O-C), and 287.9 eV (C=O) (**Figure 1D**). Compared to the high resolution C_{1s} spectrum of GO, which we reported previously, reduced intensity of peaks corresponding to oxygen-bound carbon groups particularly the C-OH/C-O-C peak was observed as a result of the reduction process[31]. Peak deconvolution yielded five peaks of rGO centred at 284.5 eV (C=C), 285.2 eV (C-C), 286.0 eV (C-OH and C-O-C), 288.5 eV (C=O), 290.7 eV (shake-up satellite) (**Figure 1F**). The relative area of each of these peaks is presented in **Table S1**. As the GO was reduced, the FWHM of the C=C peak narrowed corresponding to a more homogeneous chemical environment/restoration of the ordered structure. In addition, the percentage area of the C=C/C-C peaks relative to the total area of the C_{1s} peak increased after the reduction of GO.

Gelatin is known as a biocompatible surfactant for preparing aqueous suspensions of graphene due to the strong van der Waals and π-π stacking interactions[22, 30, 32]. Recent studies have shown that gelatin-based solutions were able to exfoliate graphene from its bulk material under sonication[30]. Therefore, the use of GelMA prevented the agglomeration of the amphiphilic rGO sheets and ensured homogeneous distribution of rGO within the hydrogel substrate. This attractive features of gelatin arise from its chemical structure. The polymeric chains of gelatin contain both hydrophilic and hydrophobic segments where the hydrophobic segments attach to the graphene surface via hydrophobic interactions[33] (**Schematic 1 B**). Gelatin has also been applied to reduce GO while stabilizing the reduced sheets in an aqueous dispersion at the same time[22]. UV-vis spectra

This article is protected by copyright. All rights reserved.

Author Manuscript

This article is protected by copyright. All rights reserved.

showed a red shift of the absorption peak from 228 nm (GO curve) to 268 nm (rGO curve) **(Figure S1)**. The red shift of 40 nm was in good agreement with the literature and can be explained by a change in electronic configuration indicating restored aromatic structures in the sheets[34].

The transmission electron microscope (TEM) images **(Figure 2A and Figure 2B)** reveal that the rGO sheets were significantly smaller than the GO sheets. Atomic force microscope (AFM) images showed that the size of the individual sheets was not uniform **(Figure 2C and Figure 2D)**. The ultrasound-driven mechanical vibrations during the preparation of the rGO solution broke the sheets into smaller pieces compared with GO. In addition, AFM analysis was conducted to investigate the thickness of the sheets of both materials. The height profile of the GO sheets showed a thickness of 1 nm **(Figure 2E)** which indicates that the GO sheets are single layer[35]. On the other hand, the thickness of the GelMA coated rGO sheets were measured to be 7 nm **(Figure 2F)**. A previous study with GelMA coated GO sheets indicated that the thickness of the GelMA coating on these carbon-based sheets were around 3 nm[36]. Given the theoretical thickness of graphene (1 nm), the rGO sheets were present as a stack of several layers as well as a GelMA coating. The agglomeration of the rGO sheets is likely due to the increased hydrophobic interactions between the individual sheets arising from the reduction step.

The rGO sheets have high absorptivity in the UV range therefore the presence of rGO sheets reduced the efficiency to produce free radicals from the photoinitiator by UV light. In addition, it is known that carbon-based materials (CNT, fullerenes, graphite) are effective free-radical

This article is protected by copyright. All rights reserved.

Author Manuscript

This article is protected by copyright. All rights reserved.

scavengers[37]. Thus, incorporation of rGO sheets in GelMA is expected to decrease the efficiency of UV-induced crosslinking. Therefore, GelMA with high degree of methacryloyl modification was chosen to provide as many methacryloyl groups as possible to promote sufficient crosslinking density in these hybrid hydrogels (**Schematic 1B**). Furthermore, a longer UV exposure time was used at higher concentrations of rGO to achieve adequate crosslinking. It is worth noting that the thickness of the hybrid hydrogel was limited by the concentration of rGO nanoparticles because the particles blocked the transmission of the UV light to the inner parts of the hydrogel scaffold. In this work, thin sheets of rGO-GelMA hybrid hydrogel (50 μm) with various concentrations of rGO from 0 mg•mL^{-1} to 5 mg•mL^{-1} were prepared by different UV exposure times (10-50 s).

Figure 3 shows the structural and electrical properties of the hybrid rGO-GelMA hydrogels. The color of the rGO films was observed to be darker when higher concentrations of the rGO particles were incoporated into the gels **(Figure 3A)**. The pore morphology of the rGO-GelMA gels was analyzed using SEM images **(Figure 3B-3E)**. Hybrid hydrogels showed a highly porous microstructure compared to pristine GelMA gels. In addition, the pore walls of hyrbid hydrogels were smooth which was an evidence for the well deispersed GelMA coated rGO particles inside the GelMA composite. The porosotiy of rGO-GelMA hydrogel decreased slightly as the rGO concentration increased from 0 mg•mL^{-1} to 3 mg•mL^{-1} (Figure S2). However, the porosity of 5 mg•mL^{-1} rGO-GelMA gel was close to that of GelMA. These observations are expected and consistent with the trend in the mechanical properties of rGO-GelMA hydrogels.

This article is protected by copyright. All rights reserved.

This article is protected by copyright. All rights reserved.

Author Manuscript

We then evaluated the Young's modulus and electrical conductivity of rGO-GelMA hydrogels at different concentrations of rGO. Force measurements on rGO-GelMA hydrogels was performed using AFM-assisted nano-indentation. The nanoindentation tests revealed that the Young's modulus increased significantly from 2.0 kPa (0 mg•mL^{-1}) to 22.6 kPa (3 mg•mL^{-1}) when all samples were crosslinked under similar conditions, suggesting that the presence of rGO nanoparticles enhanced the mechanical properties of the hydrogels **(Figure 3F)**. Interestingly, further adding more rGO nanoparticles to the hydrogel matrix did not improve its mechanical properties but rather reduced the elastic modulus of the hybrid hydrogel dramatically (12.6 kPa for 5 mg•mL^{-1}). This is attributed to the reduced crosslinking density of the films with higher rGO concentrations. To overcome this challenge, Shin et al. suggested the use of longer UV exposure times which worked quite well[13]. **Figure 3G** shows the results from the electrical conductivity measurements over a frequency spectrum of 5 orders of magnitude. The electrical impedance values were significantly lower for the samples containing rGO because of the intrinsic conductivity of the bridging rGO sheets. In addition, the rGO-GelMA hydrogels (rGO concentration of 1.0 mg•mL^{-1}) showed significantly lower impedance values (~ 4 kΩ) than those of GO-GelMA (~ 120 kΩ) and CNT-GelMA (~ 35 kΩ) gels having the same mass concentration and measured at the same frequency reported in our previous studies [13, 36].

To examine the suitability of rGO-GelMA for cell culture, NIH-3T3 cells were seeded on hydrogel films and compared with pristine GelMA. The cells formed clusters on pristine GelMA samples whereas a more homogeneous layer on the hybrid hydrogel was observed (**Figure S3A-D**). Recent

This article is protected by copyright. All rights reserved.

This article is protected by copyright. All rights reserved.

Author Manuscript

studies have shown that the incorporation of carbon-based nanomaterials into substrates having native components supported enhanced cellular adhesion due to the strong affinity between the ECM proteins and the nanomaterials[38]. rGO sheets can interact with proteins in different ways. The interaction can either be electrostatic (the remaining oxygen containing groups on the rGO sheets can be differently charged depending on the experimental conditions), π-π stacking (the sp^2 hybridized carbon atoms in the rGO sheets have delocalized electrons in the p-orbital allowing π-π interactions between the sheets and the proteins) or hydrophobic (hydrophobic parts of the proteins can interact with the hydrophobic rGO surfaces)[38]. We hypothesize that the higher cellular adhesion to the hybrid hydrogel could be due to the adsorption of more proteins onto the rGO-containing films compared to pristine GelMA hydrogels. In addition, the proliferation of the cells on the substrates were evaluated by measuring the DNA content of the cells. The increased DNA content indicated that there was no significant toxicity arising from rGO (**Figure S3E)**. To evaluate cellular viability of the rGO films, we carried out additional Live/Dead assays. We observed that there was no cytotoxicity caused by the rGO sheets as the cell viability on all the substrates was higher than 90% (**Figure S3F**).

We further evaluated the biocompatibility of the hybrid hydrogels for cardiac tissue engineering by seeding primary cardiomyocytes onto the hybrid scaffolds. The primary cardiomyocytes were isolated from neonatal rats. We found that the cellular DNA content stayed constant over a period of 9 days for all samples **(Figure 4A)** suggesting that rGO-incorporated hydrogels were not toxic to the

This article is protected by copyright. All rights reserved.

Author Manuscript

This article is protected by copyright. All rights reserved.

cardiac cells. The slight increase on day 9 for the 3 mg•mL^{-1} and 5 mg•mL^{-1} samples was possibly due to the presence of cardiac fibroblasts, left over from the isolation process. The phenotype of the cells was examined by immunostaining for the two cardiac markers of sarcomeric α-actinin and connexin 43 (Cx-43) on day 8 **(Figure 4B-E)**. Sarcomeric α-actinin is a protein related to contractile function and Cx-43 is responsible for cell-cell electrical and metabolic coupling[3]. The 2D tissues on rGO-GelMA samples showed better defined and partially uniaxially aligned sarcomeric structures compared to pristine GelMA samples. In addition, the Cx-43 was more homogeneously distributed on the rGO-GelMA constructs which is important for fast transduction of beating signals. Overall, the 2D cardiac tissues on rGO-GelMA seemed more organized with enhanced cell-cell coupling which is beneficial for improved contractile properties.

The electrophysiological properties of the engineered cardiac tissues was assessed by monitoring the spontaneous beating behavior of cardiomyocytes seeded on hybrid and pristine GelMA hydrogels. The spontaneous beating activity was recorded on a daily basis between days 4 and 7. All tissues showed spontaneous synchronous beating activity (**Figure 5A and B)**. The spontaneous beating rate was significantly higher for the 5 mg•mL^{-1} rGO-GelMA samples as compared to the pristine GelMA gels. The higher beating rates of the cardiomyocytes on rGO-GelMA hydrogels could result from a complex interplay of several factors. Mainly more uniformly distributed cardiomyocyte network and promoted maturation were obtained on rGO-GelMA, compared to the patchy cell clusters formed on pristine GelMA (**Figure 5C and D)**. The homogeneously distributed cell network

This article is protected by copyright. All rights reserved.

Author Manuscript

This article is protected by copyright. All rights reserved.

possesses uniformly distributed cell-cell junctions between neighbouring cardiomyocytes, which provide an appropriate environment for action potential propagation so that synchronized beating of cardiomyocytes was achieved throughout the cell sheet. In addition, the conductive rGO networks in GelMA hydrogel may provide additional pathways for direct electrical current flow and thus reduce the impedance for charge redistribution and action potential propagation. In previous studies, a similar mechanism was suggested for the boost of neuronal signaling on the CNT or rGO substrate.[39] Cellot and co-workers have suggested that CNTs improved electrical communications between the neurons or cardiomyocytes through the formation of tight contacts with the cell membranes.

The response of the cardiac tissue constructs to an externally applied electric field was also analyzed. Square-shaped rGO-GelMA patches spontaneously rolled up after they were detached from the glass slides. The rolling was due to the fact that cells were only seeded on one side of the patches, which resulted in a non-uniform force distribution on the sheet. Upon applying an electric field the tubes contracted along their tubular axis. **Figure 5E** shows the relaxed and contracted state of a 3 mg•mL^{-1} sample after 9 days of culture. The contraction event of the tubes could be clearly observed by naked eye (**Movie 1**). Moreover, the length of the contracted tubes was reduced by up to 12% of their original length. There was no obvious difference in contraction strengths between the samples with different rGO concentrations (1, 3 and 5 mg•mL^{-1}). The cell containing composites were stimulated at different frequencies and the rGO-GelMA constructs responded well to

This article is protected by copyright. All rights reserved.

This article is protected by copyright. All rights reserved.

Author Manuscript

frequencies of up to 3 Hz **(Figure 5F, Movie 2)**. We noticed that the beating amplitudes decreased while stimulating cells with higher stimulation frequencies because the time between two stimuli was too short for the cells to completely reach their relaxed state. In contrast to the rGO-GelMA patches, the pristine GelMA samples did not roll up but only folded and did not respond to an applied electric field. Cardiomyocytes cultured on pristine GelMA hydrogels did not form homogeneous cardiac patches and the ruptured patches were not able to generate a contracting construct.

Figure 6 shows the comparison between the function of cardiomyocytes seeded on GO-GelMA and rGO-GelMA sheets. We preapred GO-GelMA sheets according to the protocol previously developed [36]. Hybrid gels made from rGO were darker than those made from GO (**Figure 6A**). We observed that the difference between the mechanical properties of GO-GelMA and rGO-GelMA hydrogels with similar nanoparticle content (3 $mg \cdot mL^{-1}$) and GelMA concentraion (7% w/v) was insignificant (**Figure 6B**). The elastic modulus of rGO-GelMA in Figure 6B was lower than that in Figure 3F as we used a lower UV exposure time to fabricate the hydrogels. Additionally, adhesion, proliferation, and maturation of cells seeded on rGO-GelMA and GO-GelMA hydrogels were compared by culturing cardiomyocytes on hybrid hydrogels under similar conditions including nanoparticle concentration and GelMA concentration. **Fiugre 6 C and D** shows that cells covered the entire area of hydrogel surfaces homogeneously after 1 day of culture. However, the rGO-GelMA hydrogels had higher cell retention than those on GO-GelMA gels which correlated with having

This article is protected by copyright. All rights reserved.

This article is protected by copyright. All rights reserved.

Author Manuscript

higher cellular DNA contents from cells on rGO-GelMA hydrogels measured on day 1 (**Figure 6E**). Normalized DNA concentrations on day 3 by day 1 showed no significant difference between GO and rGO particle. Organization of cardiomyocytes on both hydrogels showed no significant difference after 5 days of culture under static conditions (**Figure 6 F and G**). However, we observed that the cardiomycotyes expressed more cardiac markers and showed stronger beating behavior on the rGO-GelMA hydrogels compared to the GO-GelMA hydrogels (**Figure 6 H-J**). The main reason appears to be linked to the higher electrical conductivity of rGO-GelMA hydrogels which has reduced the impedance between the cells and the substrate and promoted charge redistribution and facilited action potential propagation in the engineered tissue. Additionally, the surface physicochemical characteristics of rGO with lower oxygen containing groups and more conjugated carbon structures than GO enabled certain proteins from the culture media to be adsorbed on the rGO substrate and promoted cellular adhesion and organization[40].

3. Conclusion

In the present study, we fabricated conductive hydrogels for cardiac tissue engineering by adding rGO to the GelMA matrix. rGO was prepared by reducing GO using a naturally occurring compound (ascorbic acid), rendering the process biocompatible and less cytotoxic. The reduction of GO was confirmed with UV-vis and FTIR spectroscopy and showed that ascorbic acid is a good alternative to the commonly used toxic reducing agents like hydrazine. Electrical measurements revealed that the

This article is protected by copyright. All rights reserved.

Author Manuscript

This article is protected by copyright. All rights reserved.

conductivity of the hydrogels could be significantly increased by the incorporation of conductive rGO sheets. Furthermore, a qualitative investigation of the pore structure showed that the addition of rGO sheets to the GelMA matrix created additional pores that are beneficial for an effective diffusion of nutrients and waste products throughout the matrix. The experiments with 3T3 cells and primary cardiomyocytes demonstrate the cytocompatibility of the developed rGO-GelMA hydrogels. There was no difference in viability between cells cultured on rGO-GelMA vs. pristine GelMA scaffolds. In addition, the initial homogeneous cell attachment and spreading could be significantly improved with an increasing amount of rGO sheets in the GelMA matrix. This homogeneous cell distribution is important and essential for a proper functioning cardiac patch. Investigating the expression of cardiac markers by immunostaining showed more organized cardiomyocytes with enhanced cell-cell coupling on the rGO-GelMA hydrogels compared to the pristine GelMA samples. Moreover, the spontaneous beating rates of the cardiomyocytes seeded on rGO-GelMA hydrogels were much higher than those on GelMA gels. Furthermore, only the tissue constructs containing rGO sheets responded to an externally applied electrical field with synchronous contraction. The strong contractily activity in the rGO-GelMA constructs offers the possibility to use these hydrogel constructs for other applications such as *in vitro* drug testing. We also compared the functionality of engineered tissues made from rGO and GO based scaffolds and noticed that using rGO neither changed the mechanical property of the gels nor resulted in reduced cellular attachment. However, constructs made from rGO exhibited better cardiac function as evidenced by the expression of more cardiac markers and much higher spontaneous beating rates. Overall, our results suggest that rGO is a promising material that can be used for fabrication of tissue constructs for cardiac tissue engineering.

This article is protected by copyright. All rights reserved.

Author Manuscript

This article is protected by copyright. All rights reserved.

4. Experimental Section

Materials: Methacrylic anhydride, gelatin (Type A, gel strength 300, from porcine skin), 3-(trimethoxysily) propyl methacrylate (TMSPMA) and ascorbic acid (L-Ascorbic acid 2-phosphate sesquimagnesium salt hydrate) were purchased from Sigma-Aldrich (Wisconsin, USA). The photoinitiator, 2-hydroxy-1-(4-(hydroxyethoxy) phenyl)-2-methyl-1-propanone (Irgacure 2959) was purchased from CIBA chemical.

Synthesis of gelatin methacryloyl (GelMA): To produce the photocrosslinkable GelMA chains, gelatin was dissolved in Dulbecco's phosphate buffered saline (DPBS) (10% w/v) at 50 ^{o}C. Methacrylic anhydride (0.8 ml per gram of gelatin) was added and the mixture was stirred for 2 hours at 50 °C in order to modify lysine group on gelatin chains. To stop the methacryloyl modification reaction, the solution was diluted with DPBS. The solution was dialyzed (dialysis membrane tubings with 12 – 14 kDa molecular weight cutoff) in distilled water for 7 days at 40 °C to remove unreacted methacrylic anhydride. Afterwards, the solution was heated to 50 °C and filtrated with a vacuum filter (0.22 µm pore size). Finally, the solution was lyophilized for 7 days to obtain a dried GelMA foam. The degree of methacryloyl modification was determined by NMR spectroscopy following a previously reported method[41].

This article is protected by copyright. All rights reserved.

This article is protected by copyright. All rights reserved.

Author Manuscript

Synthesis of rGO: First, graphene oxide (GO) was synthesized from graphite according to a modified Hummers method[36]. To make rGO, 434 mg ascorbic acid (L-Ascorbic acid 2-phosphate sesquimagnesium salt hydrate, Sigma-Aldrich, USA) was dissolved in 15 mL of the GO solution (5 mg•mL^{-1}). Then, the mixture was put in a sonicator (Crest Ultrasonics, Model No 275DA, USA) for 60 min. Afterwards, the solution was kept in the oven at 80 °C for 48 hours in order to accelerate the reduction process. Then, the solution was dialyzed (dialysis membrane tubings with 12 – 14 kDa molecular weight cutoff) against distilled water for 5 days at room temperature. In order to increase the concentration of rGO in the solution, the excess water was evaporated in the oven at 80 °C. As soon as the total volume of the solution was reduced to 6 ml, the solution was removed from the oven. The remaining solution was viscous and the rGO was aggregated due to hydrophobic forces. To improve the dispersion state, 245 mg GelMA dissolved in 1.5 mL deionized water was added as a surfactant. Then, the solution was sonicated (2 s on and 1 s off, 80 W, VCX 400, Sonics, USA) for 20 min and subsequently vortexed for 5 min. The sonication and following vortexing was repeated twice. The solution was transferred to a new glass vial after letting it rest for 2 hours and the final volume was about 7 mL (some of the water evaporated during sonication due to the heat generated during the sonication procedure), which corresponds to a final GelMA concentration of 3.5%.

Preparation of rGO-GelMA hydrogel: Two different types of thin hydrogel films were produced from GO and rGO nano particles. GelMA solution (7% w/v) containing 0.5% photoinitiator was prepared, warmed up at 80 °C for 10 minutes and afterwards mixed with a selected amount of preheated GO

This article is protected by copyright. All rights reserved.

This article is protected by copyright. All rights reserved.

Author Manuscript

or rGO solution. The final target concentrations of rGO particles were 0, 1, 3 and 5 mg•mL^{-1}. To create a hydrogel thin film, 7 µL a prepolymer solution was deposited between two spacers with 50 µm height and covered with a TMSPMA-coated glass slide. The solution was then exposed to UV light (360-480 nm, 6.9 mW/cm^2) for a specific amount of time which depended on the amount of nanoparticles in the solution. The optimized crosslinking times were 6 s (0 mg•mL^{-1}), 10 s (1 mg•mL^{-1}), 60 s (3 mg•mL^{-1}) and 120 s (5 mg•mL^{-1}) for the rGO films. The gels were stored in DPBS to achieve a fully swollen state of the hydrogels.

Characterization of rGO: The absorbance of the GelMA, GO, and rGO solution were obtained with a UV spectrophotometer (Agilent, cary 100/300, USA). To test for the Fourier Transform Infrared (FTIR) spectra, the solutions were dried in an oven at 80 °C and then we obtained powders. GO and rGO powders were finely ground with KBr and compressed into pellets for FTIR measurements. The FTIR spectra were collected with a Bruker Tensor 37 FTIR spectrometer. TEM images (Tecnai 12, FEI, Netherlands) were acquired using a charge coupled detector (CCD) camera. All sample solutions were loaded onto holey-carbon film-supported grids with negative staining (Uranyl acetate). The thickness and morphology of the GelMA-coated rGO sheets was measured with AFM. The rGO dispersion was diluted to 1 mg•mL^{-1}. The excess GelMA was removed by washing the dispersion three times with preheated DPBS. Each time, the rGO sheets were collected by centrifugation at 14000 rpm for 30 min. Then, rGO and GO were placed on SiO_2 substrates pretreated with 3-amino-propyl trimethoxysilane (APTMS). The pretreatment was done by placing the dry substrates into a

This article is protected by copyright. All rights reserved.

This article is protected by copyright. All rights reserved.

Author Manuscript

dilute solution of APTMS in methanol (5% w/v) for 24 h at room temperature. Then, the substrates were rinsed throughly with methanol and treated under sonication in methanol for 5 min to remove physisorbed APTMS. Afterwards, the substrates were washed with ultrapure water and dried with N_2. Finally, the substrates were placed in an oven at 120°C for 30 min. The images were taken with an AFM (Multimode IV, Veeco, USA).

Characterization of rGO-GelMA hydrogels: Force measurements on rGO-GelMA hydrogel was performed using atomic force microscopy (AFM)-assisted nano-indentation. Briefly, this experimental setup consisted of Agilent 5500 AFM sitting on an Olympus GX71 inverted optical microscope. The spring constant of the compliant AFM cantilever was 0.20 N m^{-1} N/m, measured by Cleveland method[42], and the tip radius was estimated to be 10 nm. All the measurements were performed in PBS solution at a room temperature of 20 $^{\circ}$C. The cantilever was initially positioned above rGO-GelMA sample, and then approached and indented the sample at the rate of 1 $\mu m\ s^{-1}$. The applied load (F) was measured as a function of the position of cantilever tip. At least twenty measurements were performed for each sample with different concentrations of rGO. The measured force curves were highly reproducible. The elastic modulus (E) was derived by Hertz contact mechanics theory for spherical elastic solid:[43]

$$F = \frac{4}{3}\left(\frac{E}{1-\mu^2}\right)R^{1/2}h^{3/2} \qquad (1)$$

This article is protected by copyright. All rights reserved.

This article is protected by copyright. All rights reserved.

Author Manuscript

Where R is the radius of the cantilever tip, h is the indentation depth and μ is the Poisson's ratio of rGO-GelMA, which equals to 0.5.[44] For electrical impedance measurements, the hydrogel films were swollen in ultrapure water and then pressed between two copper electrodes. The individual impedance values were then measured for frequencies between 20 Hz and 1 MHz. The thickness of the measured films was 100 µm. The surfaces of the hydrogel films were examined using SEM (Hitachi Model S4700, Japan). Thin hydrogel films in fully swollen state were frozen by dipping them into liquid nitrogen and then kept overnight at -80°C. The samples were coated with Pt/Pd using a sputter coater. Afterwards, the samples were lyophilized and cut in half to expose their cross section prior to the imaging process.

Cell isolation and culture: Cardiomyocytes were isolated from 2-day-old Sprague-Dawley rats following a well-established protocol approved by the Institute's Committee on Animal Care [35]. The cells were then pre-plated for 1 hour to enrich the cardiomyocytes and were used immediately after. The cardiac cells were seeded onto both GelMA and rGO-GelMA samples (10 mm × 10 mm, 7.5×10^5 cells/well). The cell-seeded samples were cultured in Dulbecco's modified eagle medium (DMEM, Gibco, USA) containing 10 % fetal bovine serum (FBS, Gibco, USA), 1% L-Glutamine (Gibco, USA) and 100 units mL^{-1} penicillin-streptomycin (Gibco, USA). 3T3 fibroblasts were cultured in DMEM supplemented with 10% FBS and 1 units mL^{-1} penicillin-streptomycin and passaged every three days.

Cell characterization: The live/dead assay was performed using a staining solution containing calcein-AM (1/2000, Invitrogen) and ethidium homodimer-1 (1/500, Invitrogen) in DPBS. The samples were

This article is protected by copyright. All rights reserved.

Author Manuscript

This article is protected by copyright. All rights reserved.

immersed in the staining solution for 30 minutes at room temperature. Afterwards, the samples were washed twice with DPBS and then imaged using an inverted fluorescence microscope (Zeiss, Axio Observer.D1, Germany). The cell viability was calculated by analyzing 5 randomly chosen images from three different samples per condition with ImageJ. To do immunocytochemistry, the cells were fixed with a 4% paraformaldehyde solution for 20 minutes at room temperature. Cells were then treated with 0.1% Triton X-10 for 30 minutes to permeabilize the membrane of the cells. Samples with 3T3 cells were treated with Alexa Fluor 488 phalloidin (1:40 dilution in DPBS) and DAPI (1:1000 dilution in DPBS) for 40 minutes at room temperature. Samples with cardiomyocytes were stained with three different types of primary antibodies: for sarcomeric α-actinin, connexin 43 and Troponin I. These primary antibodies were used at 1:200 dilutions overnight at 4 °C. After the incubation with the primary antibody, the samples were treated with secondary antibody (1:200 in 10% goat serum) containing the fluorescence dye for 40 minutes at room temperature. The samples were counterstained with DAPI (1:1000 in DPBS) for 30 minutes at room temperature. Finally, the samples were imaged with an inverted laser scanning confocal microscope (Leica SP5X MP, Germany). DNA quantification was performed using PicoGreen reagent (Invitrogen) with three samples of each group. The gels were detached from the glass slide and put in an eppendorf tube containing 500 µL ultrapure water. The samples were stored at -80 °C during the sample collection period (up to 9 days). Before staining, the samples were defrosted and vortexed for 1 minute. Then, 28.7 µL of the sample solution were collected and mixed with 100 µL TE buffer (1x, Invitrogen) and 71.3 µL PicoGreen (1x) in a 96-well plate. The fluorescence signal was read using a plate reader.

This article is protected by copyright. All rights reserved.

Author Manuscript

This article is protected by copyright. All rights reserved.

Electrophysiology measurements: Each sample was monitored for spontaneous beating activity on a daily basis for the duration of the experiment with a light microscope (Nikon, Eclipse, Ti-S, Japan) using a 10x magnification. The images of the cultured cardiomyocytes were taken with a CCD camera which was attached to a microscope with a temperature control at 37 ^{o}C and the beating sequences were recorded with a video capture program. The beating sequences were analyzed using a purpose-built MATLAB code which analyzes each frame of the videos and calculates the beating frequency and draws a beating curve. The beating curve was calculated from three independent experiments with at least three gels per group in each experiment.

The response of the cardiac tissue constructs to electric field stimulation was carried out by using a platinum wire electrode system placed in a petri dish filled with cardiac media. The gels were detached from the glass slides and placed between two platinum wires in the test chamber. The electrical pulse generator (8116A, Pulse/Function Generator 50 MHz, Hewlett-Packard) produced biphasic waveforms with 50 ms pulses of 3-6 V cm^{-1} at 0.5, 1, 2 and 3 Hz.

Statistical analysis: To analyze statistical significance, we used a one-way ANOVA where appropriate (GraphPad Prism 5.02, GraphPad Software). Error bar represents the mean ± standard deviation (SD) of measurements performed on each sample group. To determine whether a significant difference exists between specific treatments, we used Tukey's multiple comparison tests ($p<0.05$).

Author Manuscript

This article is protected by copyright. All rights reserved.

This article is protected by copyright. All rights reserved.

Supporting Information: Supporting Information is available from the Wiley Online Library or from the author.

Author Manuscript

Acknowledgements

The authors acknowledge funding from the National Science Foundation (EFRI-12404433), IMMODGEL (602694), and the National Institute of Health (EB012597, AR057837, DE021468, HL099073, AI105024, AR063745).

Received: ((will be filled in by the editorial staff))
Revised: ((will be filled in by the editorial staff))
Published online: ((will be filled in by the editorial staff))

This article is protected by copyright. All rights reserved.

This article is protected by copyright. All rights reserved.

[1] V. F. Segers, R. T. Lee, Nature 2008, 451, 937; A. Alcon, E. Cagavi Bozkulak, Y. Qyang, Cell Mol Life Sci 2012, 69, 2635.

[2] K. L. Coulombe, V. K. Bajpai, S. T. Andreadis, C. E. Murry, Annu Rev Biomed Eng 2014, 16, 1.

[3] T. Dvir, B. P. Timko, M. D. Brigham, S. R. Naik, S. S. Karajanagi, O. Levy, H. Jin, K. K. Parker, R. Langer, D. S. Kohane, Nat Nanotechnol 2011, 6, 720.

[4] D. Zhang, I. Y. Shadrin, J. Lam, H. Q. Xian, H. R. Snodgrass, N. Bursac, Biomaterials 2013, 34, 5813.

[5] P. Camelliti, T. K. Borg, P. Kohl, Cardiovasc Res 2005, 65, 40.

[6] Z. Kassiri, R. Khokha, Thrombosis and haemostasis 2005, 93, 212.

[7] T. Kofidis, P. Akhyari, J. Boublik, P. Theodorou, U. Martin, A. Ruhparwar, S. Fischer, T. Eschenhagen, H. P. Kubis, T. Kraft, R. Leyh, A. Haverich, J Thorac Cardiov Sur 2002, 124, 63; M. J. Yost, C. F. Baicu, C. E. Stonerock, R. L. Goodwin, R. L. Price, J. M. Davis, H. Evans, P. D. Watson, C. M. Gore, J. Sweet, L. Creech, M. R. Zile, L. Terracio, Tissue Eng 2004, 10, 273.

[8] K. L. Christman, A. J. Vardanian, Q. Z. Fang, R. E. Sievers, H. H. Fok, R. J. Lee, J Am Coll Cardiol 2004, 44, 654; K. Yuan Ye, K. E. Sullivan, L. D. Black, Journal of visualized experiments : JoVE 2011.

[9] M. Papadaki, N. Bursac, R. Langer, J. Merok, G. Vunjak-Novakovic, L. E. Freed, Am J Physiol-Heart C 2001, 280, H168.

[10] M. Shin, O. Ishii, T. Sueda, J. P. Vacanti, Biomaterials 2004, 25, 3717.

[11] G. C. Engelmayr, M. Cheng, C. J. Bettinger, J. T. Borenstein, R. Langer, L. E. Freed, Nat Mater 2008, 7, 1003.

[12] Q.-Z. Chen, S. E. Harding, N. N. Ali, A. R. Lyon, A. R. Boccaccini, Materials Science and Engineering: R: Reports 2008, 59, 1.

[13] S. R. Shin, S. M. Jung, M. Zalabany, K. Kim, P. Zorlutuna, S. B. Kim, M. Nikkhah, M. Khabiry, M. Azize, J. Kong, K. T. Wan, T. Palacios, M. R. Dokmeci, H. Bae, X. S. Tang, A. Khademhosseini, ACS Nano 2013, 7, 2369.

[14] J. O. You, M. Rafat, G. J. Ye, D. T. Auguste, Nano Lett 2011, 11, 3643.

This article is protected by copyright. All rights reserved.

Author Manuscript

This article is protected by copyright. All rights reserved.

[15] W. Yang, P. Thordarson, J. J. Gooding, S. P. Ringer, F. Braet, Nanotechnology 2007, 18, 412001.

[16] S. R. Shin, S. M. Jung, M. Zalabany, K. Kim, P. Zorlutuna, S. b. Kim, M. Nikkhah, M. Khabiry, M. Azize, J. Kong, ACS nano 2013, 7, 2369.

[17] A. K. Geim, science 2009, 324, 1530; D. Bitounis, H. Ali‐Boucetta, B. H. Hong, D. H. Min, K. Kostarelos, Advanced Materials 2013, 25, 2258; A. Schinwald, F. A. Murphy, A. Jones, W. MacNee, K. Donaldson, ACS nano 2012, 6, 736.

[18] Y. Zhang, S. F. Ali, E. Dervishi, Y. Xu, Z. Li, D. Casciano, A. S. Biris, Acs Nano 2010, 4, 3181.

[19] X. Shi, H. Chang, S. Chen, C. Lai, A. Khademhosseini, H. Wu, Advanced Functional Materials 2012, 22, 751.

[20] Y. Zhang, S. F. Ali, E. Dervishi, Y. Xu, Z. Li, D. Casciano, A. S. Biris, ACS Nano 2010, 4, 3181.

[21] D. R. Dreyer, S. Park, C. W. Bielawski, R. S. Ruoff, Chem Soc Rev 2010, 39, 228.

[22] Y. Ge, J. Wang, Z. Shi, J. Yin, Journal of Materials Chemistry 2012, 22, 17619.

[23] I. Kanayama, H. Miyaji, H. Takita, E. Nishida, M. Tsuji, B. Fugetsu, L. Sun, K. Inoue, A. Ibara, T. Akasaka, T. Sugaya, M. Kawanami, Int J Nanomedicine 2014, 9, 3363.

[24] L. Jin, D. Wu, S. Kuddannaya, Y. Zhang, Z. Wang, ACS Appl Mater Interfaces 2016, 8, 5170.

[25] M. Patel, H. J. Moon, Y. Ko du, B. Jeong, ACS Appl Mater Interfaces 2016, 8, 5160.

[26] A. A. Oun, J. W. Rhim, Carbohydr Polym 2015, 127, 101.

[27] M. J. Fernandez-Merino, L. Guardia, J. I. Paredes, S. Villar-Rodil, P. Solis-Fernandez, A. Martinez-Alonso, J. M. D. Tascon, J Phys Chem C 2010, 114, 6426; J. L. Zhang, H. J. Yang, G. X. Shen, P. Cheng, J. Y. Zhang, S. W. Guo, Chem Commun 2010, 46, 1112.

[28] Z. J. Guan, C. Y. Lui, E. Morkin, J. J. Bahl, J Cardiovasc Pharm 2004, 44, 696; T. Takahashi, B. Lord, P. C. Schulze, R. M. Fryer, S. S. Sarang, S. R. Gullans, R. T. Lee, Circulation 2003, 107, 1912; M. Fernandez-Merino, L. Guardia, J. Paredes, S. Villar-Rodil, P. Solis-Fernandez, A. Martinez-Alonso, J. Tascon, The Journal of Physical Chemistry C 2010, 114, 6426; J. Zhang, H. Yang, G. Shen, P. Cheng, J.

This article is protected by copyright. All rights reserved.

Author Manuscript

This article is protected by copyright. All rights reserved.

Zhang, S. Guo, Chemical Communications 2010, 46, 1112; Z. Guan, C. Y. Lui, E. Morkin, J. J. Bahl, Journal of cardiovascular pharmacology 2004, 44, 696.

[29] M. Nikkhah, N. Eshak, P. Zorlutuna, N. Annabi, M. Castello, K. Kim, A. Dolatshahi-Pirouz, F. Edalat, H. Bae, Y. Yang, A. Khademhosseini, Biomaterials 2012, 33, 9009.

[30] K. Liu, J.-J. Zhang, F.-F. Cheng, T.-T. Zheng, C. Wang, J.-J. Zhu, Journal of Materials Chemistry 2011, 21, 12034.

[31] X. Gao, X. Tang, Carbon 2014, 76, 7.

[32] C. Shan, H. Yang, D. Han, Q. Zhang, A. Ivaska, L. Niu, Langmuir 2009, 25, 12030.

[33] S. R. Shin, H. Bae, J. M. Cha, J. Y. Mun, Y.-C. Chen, H. Tekin, H. Shin, S. Farshchi, M. R. Dokmeci, X. Tang, A. Khademhosseini, ACS Nano 2012, 6, 362.

[34] D. Li, M. B. Muller, S. Gilje, R. B. Kaner, G. G. Wallace, Nature Nanotechnology 2008, 3, 101.

[35] C. Shan, H. Yang, D. Han, Q. Zhang, A. Ivaska, L. Niu, Langmuir 2009, 25, 12030.

[36] S. R. Shin, B. Aghaei-Ghareh-Bolagh, T. T. Dang, S. N. Topkaya, X. Gao, S. Y. Yang, S. M. Jung, J. H. Oh, M. R. Dokmeci, X. S. Tang, A. Khademhosseini, Advanced Materials 2013, 25, 6385.

[37] A. Galano, Journal of Physical Chemistry C 2008, 112, 8922.

[38] Y. XZhang, C. Wu, S. Guo, J. Zhang, Nanotechnology Reviews 2013, 2, 18.

[39] V. Lovat, D. Pantarotto, L. Lagostena, B. Cacciari, M. Grandolfo, M. Righi, G. Spalluto, M. Prato, L. Ballerini, Nano Lett 2005, 5, 1107.

[40] X. Shi, H. Chang, S. Chen, C. Lai, A. Khademhosseini, Advanced Functional Materials 2012, 22, 751.

[41] J. W. Nichol, S. T. Koshy, H. Bae, C. M. Hwang, S. Yamanlar, A. Khademhosseini, Biomaterials 2010, 31, 5536.

[42] J. P. Cleveland, S. Manne, D. Bocek, P. K. Hansma, Review of Scientific Instruments 1993, 64, 3.

Author Manuscript

This article is protected by copyright. All rights reserved.

This article is protected by copyright. All rights reserved.

[43] P. A. L. Fernandes, S. Schmidt, M. Zeiser, A. Fery, T. Hellweg, Soft Matter 2010, 6, 4.

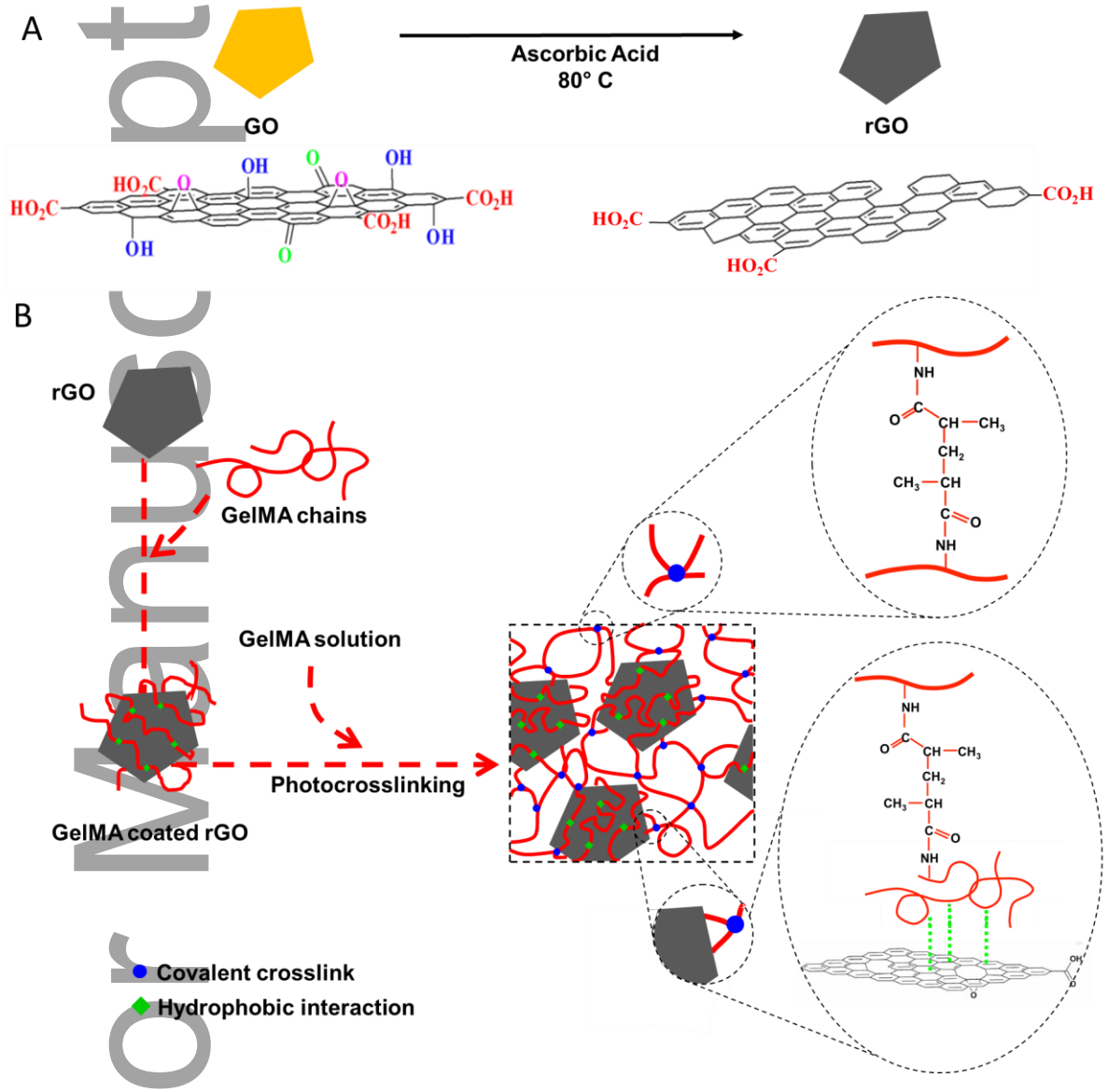
[44] M. Ahearne, Y. Yang, A. J. El Haj, K. Y. Then, K. K. Liu, J R Soc Interface 2005, 2, 455.

Author Manuscript

This article is protected by copyright. All rights reserved.

This article is protected by copyright. All rights reserved.

FIGURE CAPTIONS.



Author Manuscript

This article is protected by copyright. All rights reserved.

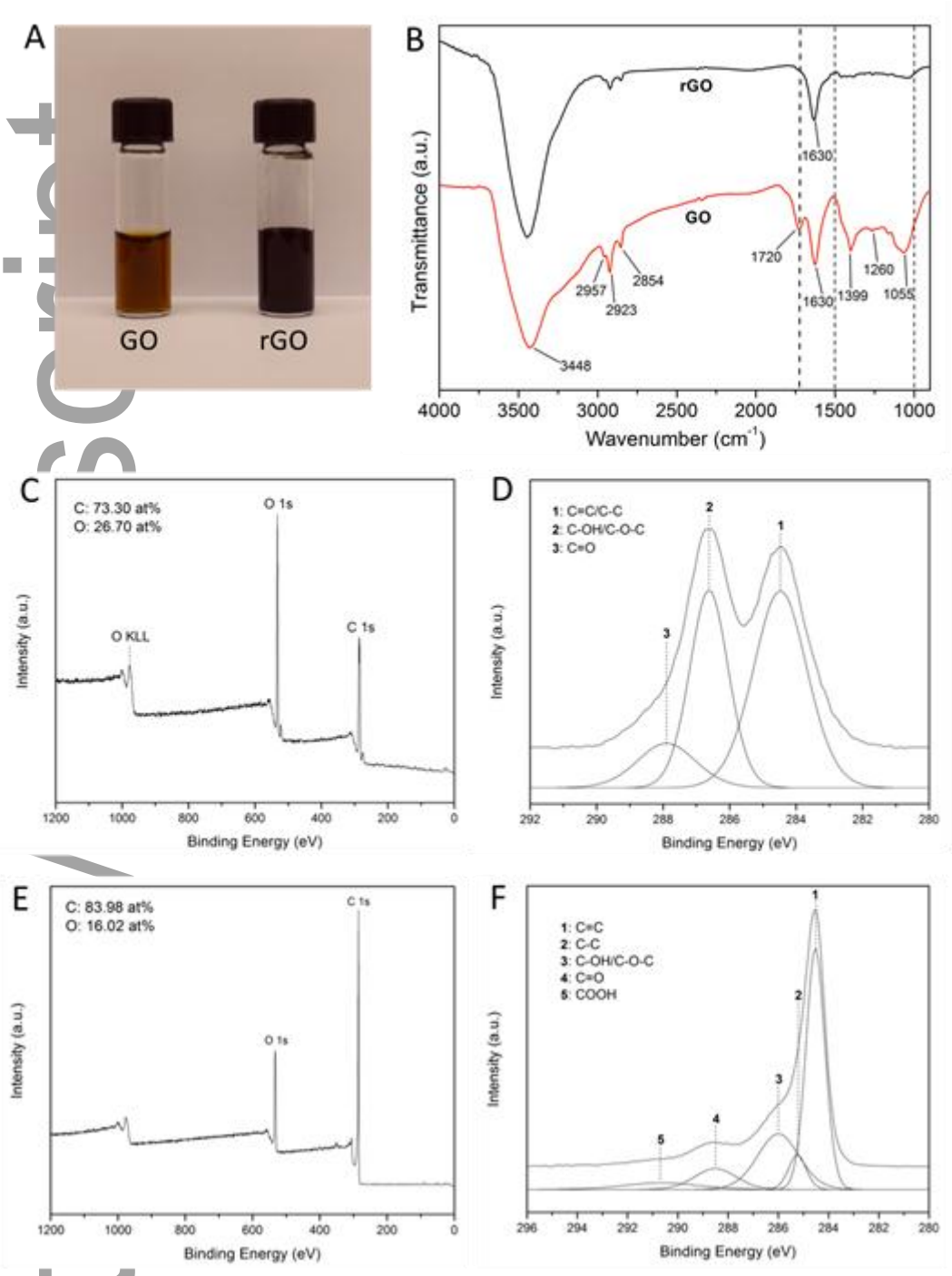
This article is protected by copyright. All rights reserved.

Schematic 1. Schematic illustration of the rGO-GelMA synthesis process. (A) Process of producing rGO from GO using ascorbic acid. (B) Preparation procedure of rGO-GelMA hybrid hydrogels.

Author Manuscript

This article is protected by copyright. All rights reserved.

This article is protected by copyright. All rights reserved.



This article is protected by copyright. All rights reserved.

This article is protected by copyright. All rights reserved.

Figure 1. **Chemical characterization of the GO and rGO nanoparticles.** (A) An optical image of GO and rGO dispersions. The initial brownish color of the GO solution changed to black after the reduction process. (B) FTIR spectra of GO and rGO. XPS spectra of (C & D) GO and (E & F) rGO.

Author Manuscript

This article is protected by copyright. All rights reserved.

This article is protected by copyright. All rights reserved.

Author Manuscript

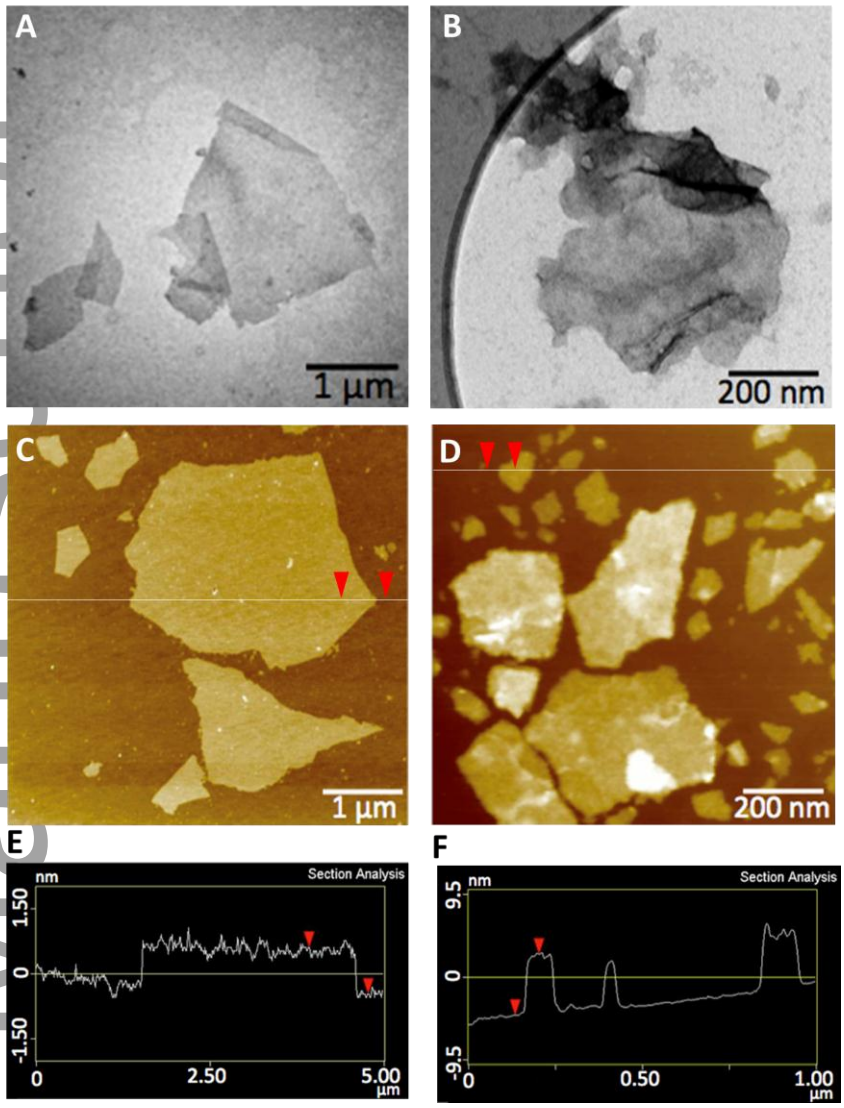


Figure 2. Physical characterization of the GO and rGO nanoparticles. TEM images of (A) GO and (B) rGO sheets. AFM images of (C) GO and (D) GelMA coated rGO. (E & F) The height profile along the indicated line in images (C) & (D) respectively.

This article is protected by copyright. All rights reserved.

This article is protected by copyright. All rights reserved.

Author Manuscript

This article is protected by copyright. All rights reserved.

This article is protected by copyright. All rights reserved.

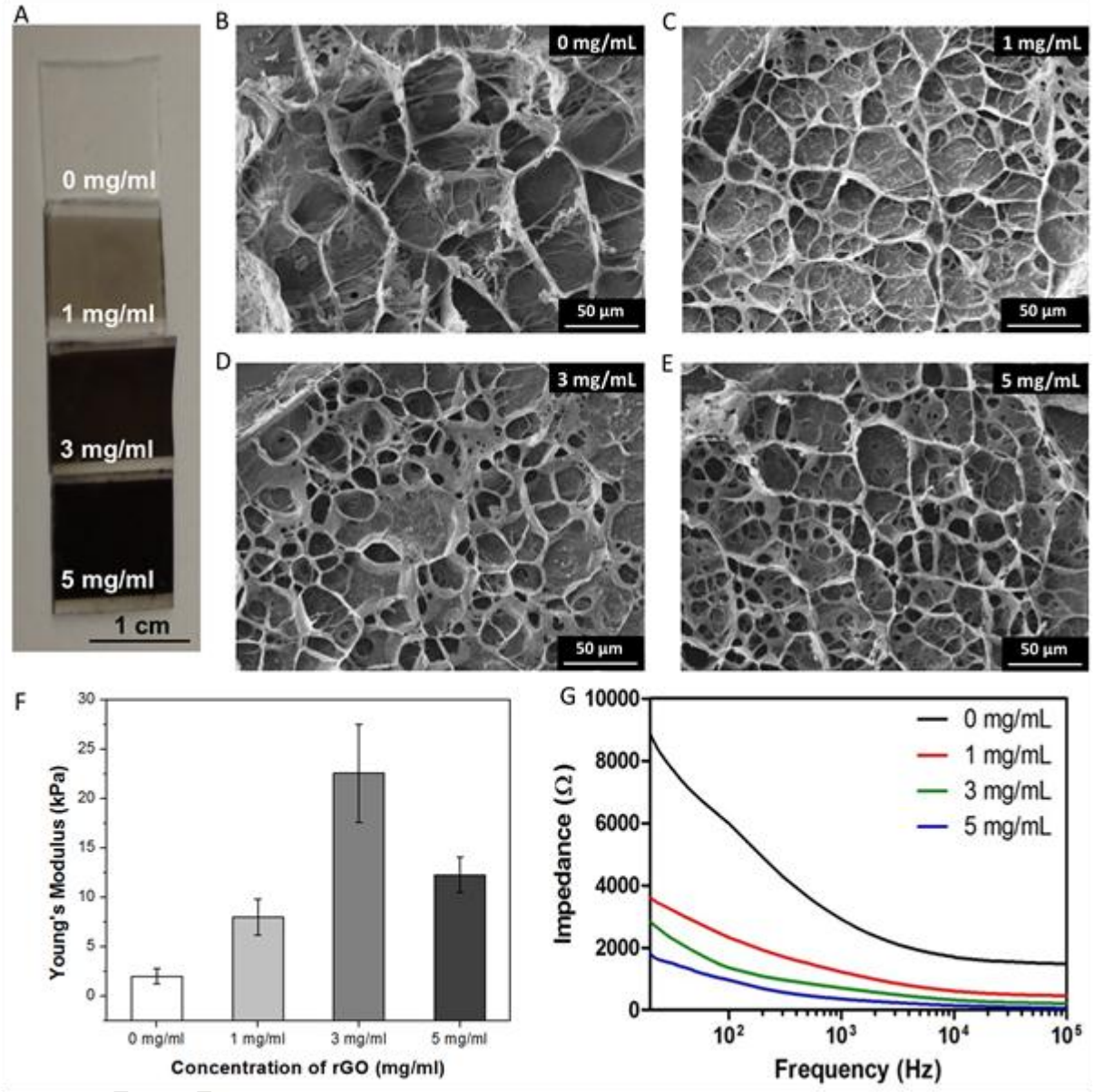


Figure 3. Structural and electrical properties of pristine GelMA and rGO-GelMA hydrogels. (A) Optical images and (B-E) SEM images of rGO-GelMA hydrogels with various concentrations of rGO: 0,

This article is protected by copyright. All rights reserved.

This article is protected by copyright. All rights reserved.

1, 3 and 5 mg• mL^{-1}. The overall porosity of the gel were found to increase with increasing rGO concentration. (F) The elastic modulus of rGO-GelMA under compression at fully swollen state varies significantly with rGO concentration (*$p < 0.05$). (G) Electrical impedance curves of rGO-GelMA hydrogels with various concentrations of rGO. The impedance values were significantly lower for the samples containing rGO due to the good intrinsic conductivity of the bridging rGO sheets.

Author Manuscript

This article is protected by copyright. All rights reserved.

This article is protected by copyright. All rights reserved.

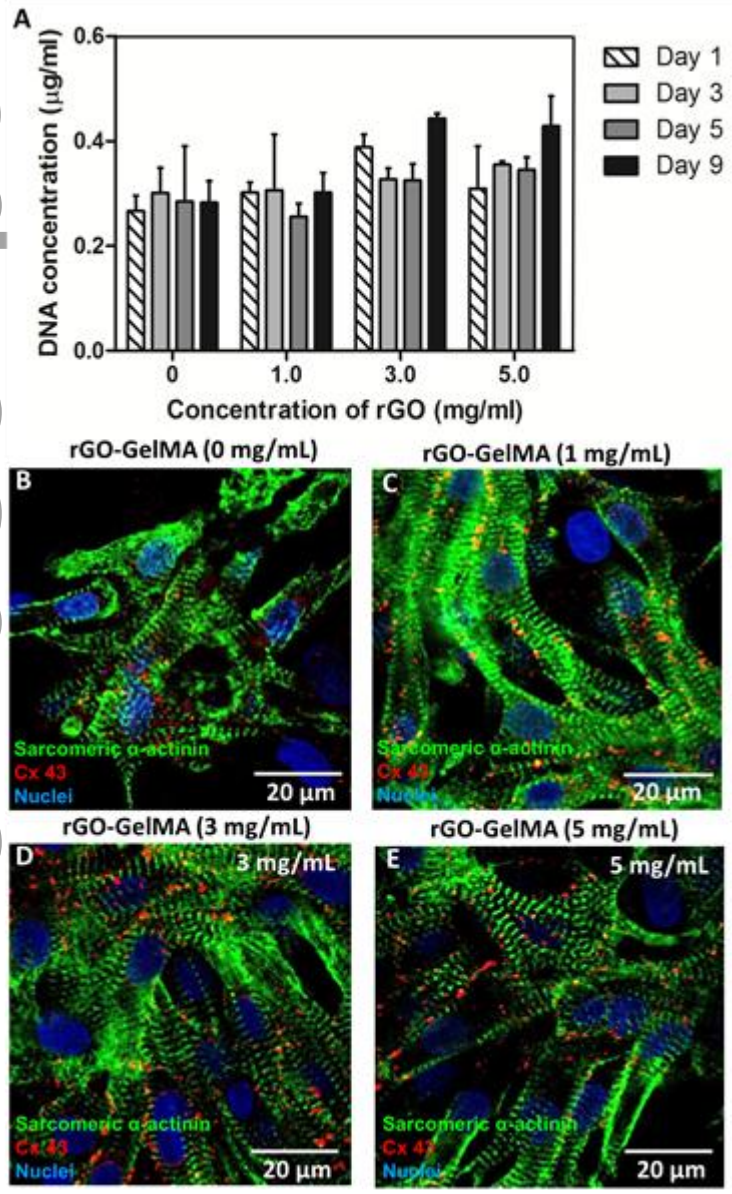


Figure 4. Phenotype of cardiac cells on pristine GelMA and rGO-GelMA hydrogels. (A) Cellular DNA content of cardiomyocytes on days 1, 3, 5, and 9 after seeding (n=4, avg±SD). The cellular

This article is protected by copyright. All rights reserved.

Author Manuscript

This article is protected by copyright. All rights reserved.

DNA content stayed relatively constant over a period of 9 days in all samples. (B–E) Images of cardiomyocytes immunostained for cardiac markers on day 8: sarcomeric α-actinin (green), connexin 43 (red), nucleus (blue). Four different concentrations of rGO are shown: (B) 0 mg• mL^{-1}, (C) 1 mg• mL^{-1}, (D) 3 mg• mL^{-1}, (E) 5 mg• mL^{-1}. The 2D tissues on rGO-GelMA samples showed well-defined and more uniaxially aligned sarcomeric structures and more homogeneously distributed Cx-43, compared to those on pristine GelMA samples.

Author Manuscript

This article is protected by copyright. All rights reserved.

This article is protected by copyright. All rights reserved.

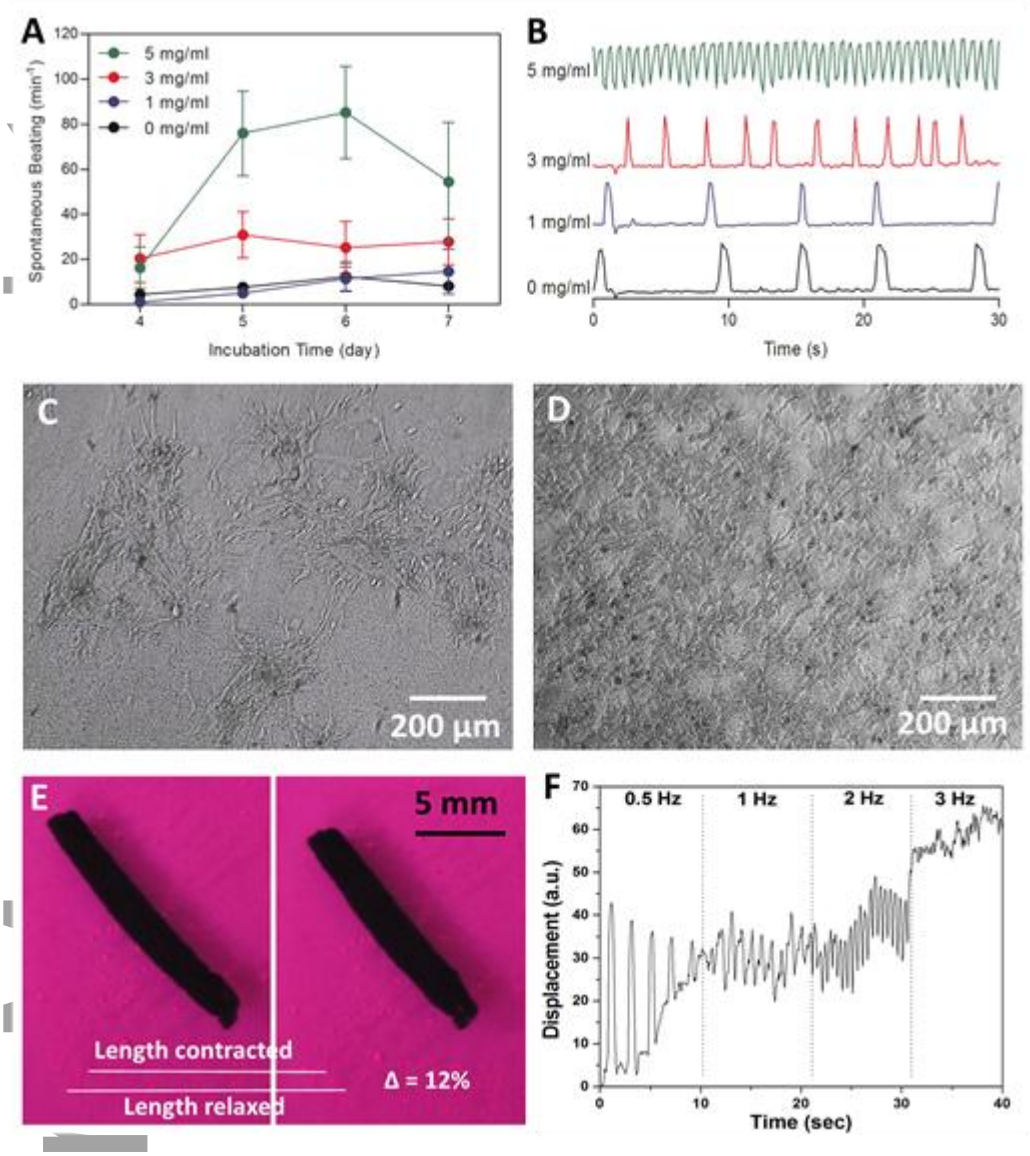


Figure 5. Electrophysiological properties of the engineered cardiac tissues. (A) Spontaneous beating rates of cardiomyocytes seeded on pristine GelMA (0 mg•mL^{-1}) and rGO-GelMA (1, 3, 5 mg•mL^{-1}) hydrogels as a function of incubation time. (B) Beating patterns of cardiomyocytes recorded

This article is protected by copyright. All rights reserved.

This article is protected by copyright. All rights reserved.

on day 6 on rGO-GelMA hydrogels**.** Phase contrast images showing cultured cardiomyocytes (C) on pristine GelMA and (D) on 3 mg•mL^{-1} rGO-GelMA substrates 6 days after seeding. (E) Optical images show the relaxed (left) and contracted (right) cardiac tissue constructs cultured on a 3 mg•mL^{-1} rGO-GelMA sample stimulated using an external electrical field. (F) Response of a 3 mg•mL^{-1} rGO-GelMA tissue sample to an applied external electrical field at various frequencies (0.5, 1 and 2 Hz).

Author Manuscript

This article is protected by copyright. All rights reserved.

This article is protected by copyright. All rights reserved.

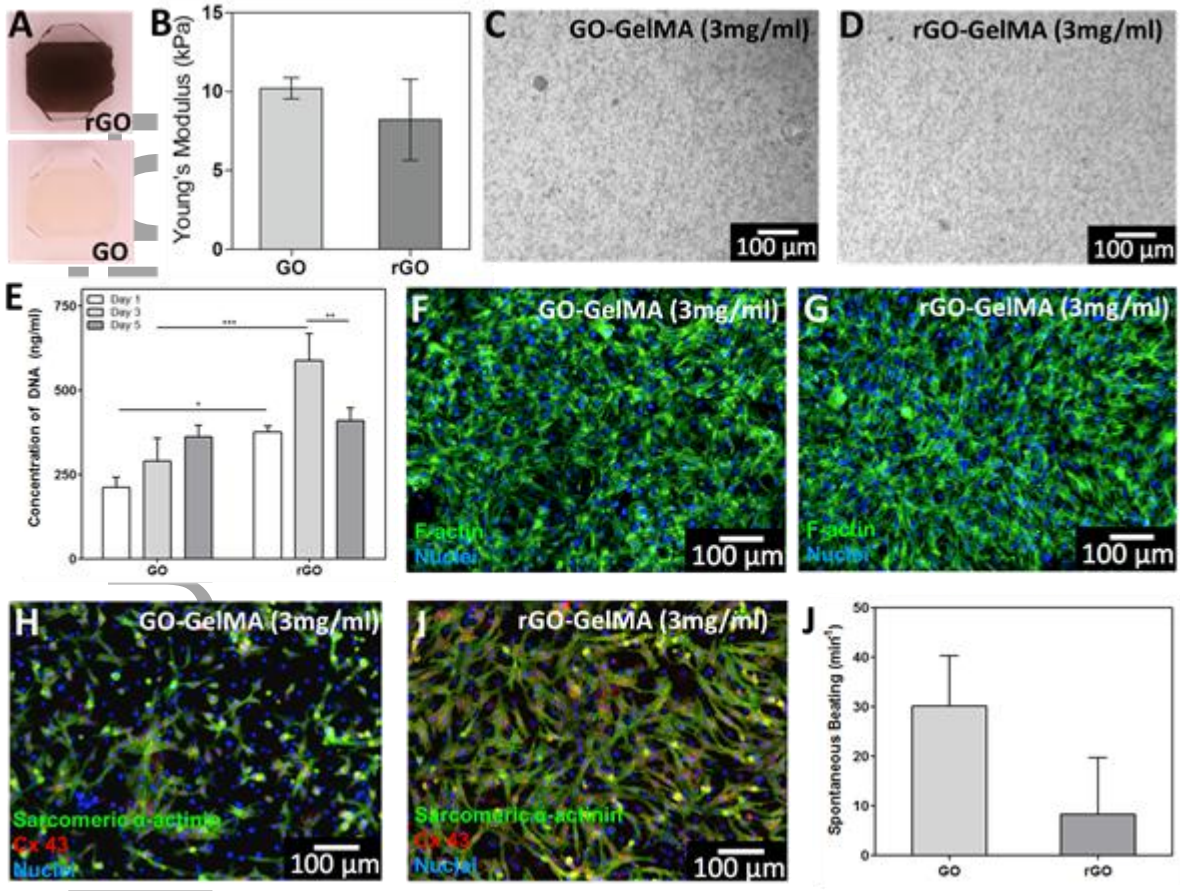


Figure 6. Function of cardiac tissues on of GO and rGO hybrid hydrogel. (A) Optical images of rGO- and GO-GelMA hydrogels with 3 mg•mL^{-1} rGO or GO respectively. (B) The elastic modulus of rGO- and GO-GelMA hydrogels under compression at fully swollen state. Phase contrast images showing cardiomyocytes on day 6 post seeding: (C) on GO-GelMA and (D) on rGO-GelMA. The more homogeneously distributed and aligned cardiomyocytes on the rGO-GelMA hydrogels allowed the formation of a well-organized cell sheet. (E) Cellular DNA content of cardiomyocytes on days 1

This article is protected by copyright. All rights reserved.

Author Manuscript

This article is protected by copyright. All rights reserved.

and 3 after seeding (n=4, avg±SD). The cellular DNA content stayed relatively constant over a period of 5 days in all samples. (*$p < 0.05$, **$p < 0.001$) Immunostaining of f-actin (green) and nucleus (blue) on day 2 after cell culture showed cardiomyocyte adhesion and spreading on (F) GO- and (G) rGO-GelMA hydrogel surfaces. Images of cardiomyocytes immunostained for cardiac markers with sarcomeric α-actinin (green), Cx-43 (red), and nuclei (blue) on (F) GO- and (G) rGO-GelMA hydrogels (day 8 of culture). (J) Spontaneous beating rates of cardiomyocytes seeded on GO- and rGO-GelMA hydrogels on day 5.

Author Manuscript

This article is protected by copyright. All rights reserved.

This article is protected by copyright. All rights reserved.